First-principles molecular dynamics compression of small metallic nanoparticles

Laurent Pizzagalli, J. Durinck, S. Brochard, J. Godet

First-principles molecular dynamics compression of small metallic nanoparticles

L. Pizzagalli[a,*], J. Durinck[a], S. Brochard[a], J. Godet[a]

[a]*Institut P′, CNRS UPR 3346, Université de Poitiers, SP2MI, Boulevard Marie et Pierre Curie, TSA 41123, 86073 Poitiers Cedex 9, France*

Abstract

Whether the strength of materials keeps increasing, saturates or decreases when characteristic dimensions are reduced down to the nanometer scale remains an open question. To bring new insights, first principles molecular dynamics calculations are performed to model the compression of 1–2 nm aluminum nanoparticles with different shapes. We find that the plastic deformation occurs at high strains and stresses by a mechanism combining diffusive and displacive atomic displacements. This deformation mode is characterized by a slow dynamic and the partial or even complete recovery of crystalline order. The strength depends on the nanoparticles shape, and is in all cases significantly higher than the theoretical bulk strength. It is however substantially lower than values extrapolated using reported classical molecular dynamics investigations. Our results suggest that the strength saturates at low scales.

Keywords: Compression test, Nanostructure, Aluminum, First-principle calculation, Molecular dynamics

Since the pioneering works by Taylor [1] and Brenner [2], we know that the strength of metals can be several orders of magnitude higher than in the bulk when samples dimensions are significantly reduced. Recently, Rabkin and collaborators demonstrated that it is even possible to reach the theoretical strength, an intrinsic property of material which can be determined using ab initio calculations [3], when compressing Ni [4] and Mo [5] nanoparticles (NP) with sizes of a few hundreds of nanometers. The strength seems to reach a plateau when sizes are further reduced, at least for iron NP [6]. Ultimately, Azadehranjbar et al. showed that platinum NP becomes weaker under compression for decreasing sizes in the range 9–41 nm [7], because of the dominant role of surface diffusion at low scales and room temperature.

Compression experiments at the nanoscale are difficult to perform, and results are prone to uncertainties. One additional complexity is the influence of shape on mechanical properties at small sizes [5, 8–10]. Molecular dynamics (MD) simulations are an interesting alternative to experiments, with a full control of NP models and simulation conditions [11]. However they are limited to short timescales, which prevents their use for describing diffusive mechanisms at play for small NP and ambient conditions. It explains why most available simulation studies focus on low temperatures at 10 K or below, for which thermally activated surface diffusion is negligible. In the case of FCC NP, classical MD calculations reveal that the strength increases according to a power law relation when the size decreases from 80 nm to 5 nm, with a dislocation-mediated plasticity [12–14].

An intriguing and unanswered question is how strength varies when the NP size is further decreased? Extrapolations using published power law relations lead to extremely high values of 50 GPa (Al) and 80 GPa (Ni) for 1 nm NP [12], much larger than the theoretical strength of the respective bulks. Such values obviously call for further validation, especially since classical MD calculations rely on the use of interatomic potentials which are often not designed to model accurately surfaces and highly strained materials, two critical aspects of small NP compression. To circumvent this issue and obtain meaningful answers, we perform ab initio molecular dynamics (AIMD) to simulate the compression of Al NP in the size range 1–2 nm. Aluminum is selected here because of its reduced computational cost in AIMD calculations compared to other FCC metals, and the availability of data from classical MD simulations [12, 14]. We focus on strength and plasticity mechanisms, and consider the influence of NP shapes.

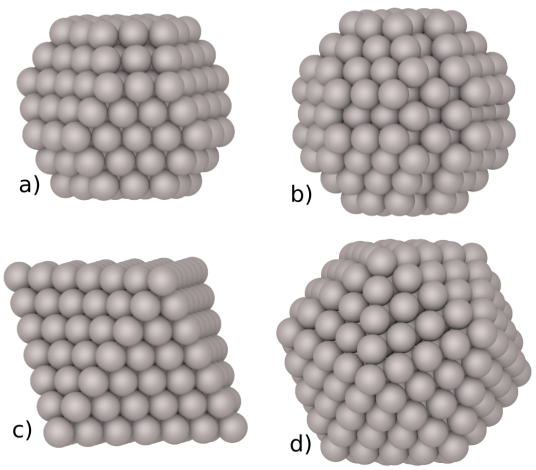

Figure 1: Examples of investigated nanoparticle models: a) Wulff (W201), b) sphere (S236), c) octahedron (O231), d) icosahedron (I309). Compression axis is vertical in this figure.

*Corresponding author: Tel: +33 549497499. E-mail: Laurent.Pizzagalli@univ-poitiers.fr

AIMD calculations are performed using the Quantum Espresso code [15]. Conversely to previous similar compression simulations [16–18], a Born-Oppenheimer framework is used for dynamics since it is more efficient for metallic systems. Electronic structure calculations are made in supercells large enough to ensure a minimum vacuum distance of 10 Å between NP replicas. An excellent compromise between accuracy and performance is obtained using a 30 Ry plane wave cutoff, a γ-point sampling, 1st-order Methfessel-Paxton smearing [19] and the PBE exchange-correlation functional [20]. Core electrons are taken into account in the framework of the projector-augmented wave method [21].

The compression of NP is achieved by means of combining AIMD calculations with planar repulsive classical force fields. This original approach allows ignoring flat punch indenters into electronic structure calculations, thus making feasible the latter using current high performance computation resources. The method is fully described in Ref. [22], and only general principles are recalled here. Two planar force fields, sandwiching the NP, are moved closer along the compression direction with a speed of 0.05 Å ps^{-1}, yielding an indentation velocity of 0.1 Å ps^{-1} similar to values used in classical investigations [11]. In the present study a force field strength parameter of 1836 eV Å^{-3} is used, which mimics incompressible flat-punch indenters. A typical compression simulation requires about 6×10^3 AIMD steps, corresponding to a total duration of 30 ps. The temperature is set at 1 K and controlled thanks to a velocity-rescaling thermostat [23]. The advantages of using a low temperature are: (i) the well known strain rate issue of simulations is largely mitigated [24], (ii) diffusion plasticity, experimentally reported at higher temperatures [7, 25], is suppressed, (iii) a meaningful comparison with previous classical MD calculations of NP compression, also performed at low temperatures [12–14].

We consider NP with various shapes like Octahedron (O), Wulff-like (W) and sphere (S), which are all energetically stable and exhibit well defined {111} facets (Fig. 1). The W NP are generated using the surface energies reported by Wan et al. [26]. Icosahedral-type (I) NP, shown as low energy configurations for Al clusters and characterized by the absence of FCC stacking [27], are also studied for comparison (Fig. 1). These models are first relaxed until forces are lower than 0.026 eV Å^{-1}. They are next oriented so as to get the compression axis normal to {111} facets. In the following, NP are named according to their shape and their number of atoms (Fig. 1).

The total energy and the forces applied by the force fields are recorded during all compression tests. The contact stress is calculated by dividing the applied force by the contact surface at each step. To obtain the latter, we first determine NP atoms less than 0.1 Å away from the force field position along the compression axis. The area S_0 of the 2D convex hull built from these atoms can be used as a first guess of the contact surface. However using S_0 yields unrealistically high stress values for small NP because contributions from surface edge atoms are underestimated. Corrections have been proposed to better account for edge atoms surface, using atomically-defined quantities [18, 28]. In the present work, we adopt an even more conservative approach by postulating that the projected surface of an atom is equal to s_{111}, the area per atom of a {111} surface. Assuming a regular polygonal shape for the contact surface, we calculate the corrected contact surface $S = S_0 + (m/2 + 1)s_{111}$, with m the number of edge atoms. Within this definition S can be considered an upper limit of the contact surface. Finally the engineering strain ε is defined relatively to the difference between force field positions, with an origin corresponding to applied forces departing from zero.

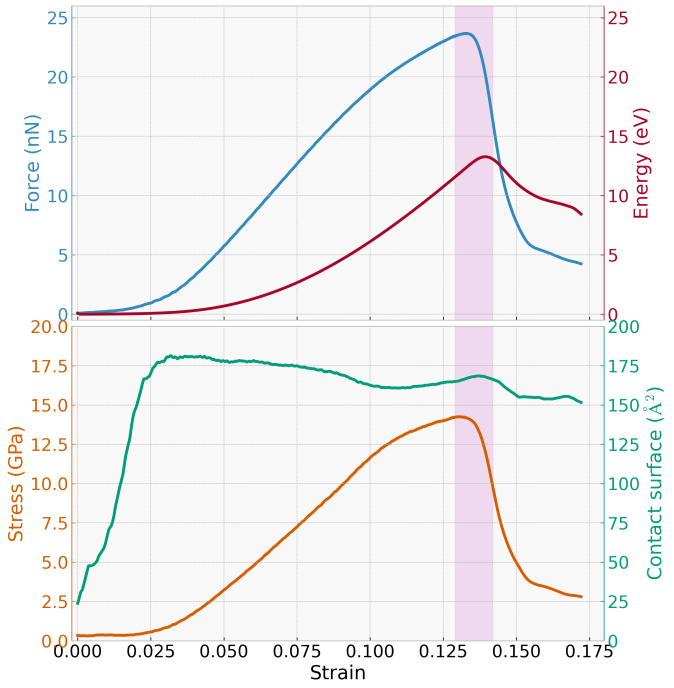

Figure 2: Force (nN, blue), energy (eV, red), stress (GPa, orange), and contact surface (Å^2, green) as a function of engineering strain, for the compression of O231. The pink strip marks the strain range for which plastic deformation occurs.

The applied force, energy, and contact stress calculated during the compression of O231 are shown in Fig. 2. All quantities increase with the strain, first weakly up to $\varepsilon = 0.02$ then markedly with seemingly linear (force and stress) or quadratic (energy) variations. The first stage is associated with a significant increase of the contact surface (Fig. 2) due to the progressive flattening of the indented facets, which are initially slightly curved after the initial relaxation. At a strain $\varepsilon \simeq 0.10$ both force and stress curves soften. A similar behavior is observed during the compression of bulk aluminum [29]. Maxima are reached at a strain $\varepsilon_y = 0.135 - 0.140$, first for force/stress, and next for energy, marking the end of the elastic stage and the initiation of plastic deformation. Maxima are followed by large but gentle decreases. This is substantially different from sharp drops associated with dislocation nucleation/propagation in larger NP [12], and suggests a slow and stress-driven plastic deformation.

Curves for O, S and W nanoparticles share similar characteristics, albeit with minor differences for the strain ranges of each stage. For instance, indented facets for W and S are ini-

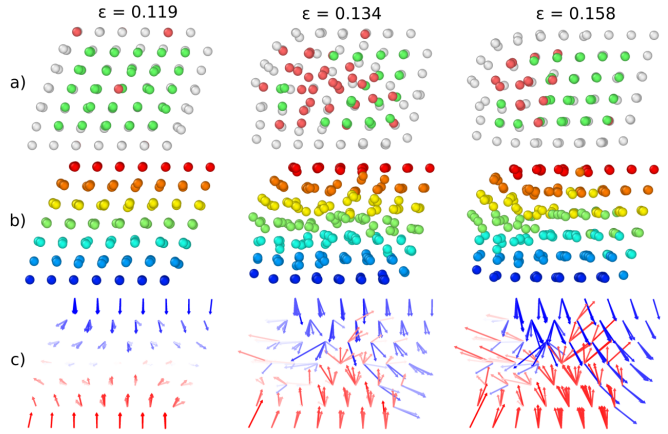

Figure 3: Side views of O231 at different compression strains (compression axis vertical to the figure). a) Atoms are represented by spheres colored using the polyhedral template matching method [30] (green: FCC atoms, red: HCP atoms, white: unknown structure). A cross section is made to see the NP inside. b) Atoms are represented by spheres colored according to their zero-strain positions along the compression axis. c) Cumulative atomic displacements (relatively to $\varepsilon = 0$) are shown as colored arrows centered on atomic positions. The arrows color depends on the z-component of the displacement.

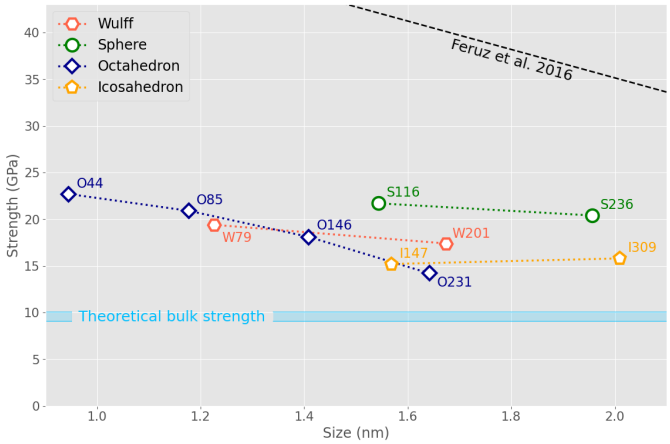

Figure 4: Strength (GPa) versus size (nm) plots for Al nanoparticles (Wulff: red hexagons, sphere: green circles, octahedron: dark blue losange, icosahedron: orange pentagons). The light blue strip shows the theoretical bulk strength range. The dashed black line represents values extrapolated from Ref. [12].

tially almost planar, with a short and limited flattening stage. We also note that ε_y is remarkably always in the range 0.13-0.14 for O, W, S and I147 NP. Only for I309 plasticity occurs at a slightly lower strain $\varepsilon_y \simeq 0.12$.

In most cases the plastic deformation is associated with the displacement of a large proportion of the NP atoms, mainly located in the central {111} planes perpendicular to the compression axis. This mechanism can be identified as diffusion under stress but with a variable degree of correlation between neighboring atoms. To better illustrate this concept, several steps during the deformation of O231 are represented in Fig. 3 (A full movie is also available in Supp. Mat.). At a strain $\varepsilon = 0.119$, i.e. right before the onset of plasticity, the FCC stacking is preserved, although one can note slight distortions, lateral NP expansion, and non homogeneous deformations (Figs. 3-b,c). By increasing the strain, atoms in center planes tend to mix in a seemingly random fashion. A close inspection of cumulative atomic displacements however reveals a partial correlation between neighboring atoms as well as migration directions mainly contained in tilted {111} planes. This corresponds to an increase of atoms in a HCP local environment. At $\varepsilon = 0.158$ the NP structural transformation is complete, with a transition from n to $n-1$ {111} planes along the compression axis, and the mixing of atoms in the center planes. Interestingly, the FCC stacking is largely recovered although residual disorder can be observed in a limited region.

A similar scenario is identified for the other NP with FCC stacking, with variations in displacement correlations and in residual disorder. The highest degree of correlation is observed for S236. In that case, one half of the NP glides along a tilted {111} plane, i.e. it corresponds to the formation and propagation across the NP of a dislocation in a {111} plane. The lowest proportion of residual disorder is obtained for O44, O85, and S116, while Wulff-like NP exhibit the most disordered final structures. Finally, the plastic deformation of icosahedral NP results in the disordered failure of one of the contact surfaces, while no irreversible displacements are observed in the NP center (see movies in Supp. Mat.). This could be explained by the lack of {111} planes in these NP.

A noteworthy feature in all cases is the wide strain range over which the plasticity mechanisms are at work. This is in sharp contrast with larger NP yielding by dislocation avalanches [11, 12, 31], which highlights the specific and original mechanical properties of small FCC NP. The gentle and progressive stress relaxation is partly due to the diffusion under stress character of the plastic deformation. It also suggests that the yield path in configuration space is characterized by wide and low energy barriers, which is characteristic of mechanisms with large activation volume. In fact, we note that a large proportion of atoms is significantly displaced during plastic deformation, hinting that the activation volume is of the same order of magnitude than the NP volume.

The strength values, defined as the maximum stress at the onset of plasticity, are reported in Fig. 4 for all investigated NP. A striking feature is the very high strength in all cases. As previously mentioned, we carefully checked that this is not caused by an underestimation of the contact surfaces. For instance, we find that S116 and S236 are significantly stronger than W79, I147, or I309 although their contact surface areas at yield are similar. Small NP also seem to be stronger than large ones for a given shape, except for icosahedron, but additional data would be needed to be more conclusive. Overall, we find that there is a clear influence of shape on strength, in agreement with previous works at larger scales [8, 9, 11]. To our knowledge, this aspect remains largely unexplained in literature. Mordehai et al. proposed that the initiation of plasticity is intimately related to stress gradients in the vicinity of contact surface edges [32]. The NP shape may influence the localization and the magnitude of stress inhomogeneities, and thus the threshold stress to activate plasticity mechanisms.

It is also interesting to compare our results with the theo-

retical strength of bulk aluminum. First principles calculated values for the ⟨112⟩{111} slip system range from 2.84 GPa to 3.16 GPa [33–35]. With a Schmid factor of 0.314 for a ⟨111⟩ compression, this corresponds to a theoretical bulk strength range of 9.04–10.06 GPa. All our data are significantly higher for all sizes and shapes (Fig. 4). This can be partly explained by predictions of a significant hardening of bulk Al when subjected to a normal stress along ⟨111⟩ [33]. For the smallest NP, one also cannot exclude a possible quantum confinement effect [27]. Finally, we note that decreasing the dimensions increases the influence of surfaces and the stability of amorphous configurations relatively to the crystalline phase, a well established result [36]. Our calculations reveal distortions in atomic positions at large strains, in agreement with a lesser stability of the crystalline order. Such distortions might inhibit the correlated displacements of atoms, thus delaying the onset of plasticity and increasing the strength.

One motivation of this work was to check the validity at low scales of strength–size relations obtained from classical MD calculations. In particular Feruz and Mordehai determine that the strength of Al Wulff-like NP compressed along ⟨111⟩ is $\sigma_c = 49.16R^{-0.512}$ for sizes between 5 nm and 30 nm. Figure 4 shows stresses extrapolated at smaller sizes using this relation, which are roughly twice as high as our values. Such a large difference can hardly be explained by minor technical differences between investigations. It is possible that the Feruz relation was not valid at low scales since it relies on calculations made with classical potentials, probably not accurate enough to describe highly strained small NP. Another explanation is that the NP strength stops increasing for sizes below 5 nm, with only small variations depending on shape. A similar behavior is proposed for Fe [6] and Ni [4] NP, albeit with different size transitions and NP shapes.

In summary, using an original approach combining first-principles molecular dynamics calculations and repulsive force fields, we find that aluminum NP with sizes 1–2 nm yield at very high stresses during a ⟨111⟩ compression. The plastic deformation corresponds to a combination of diffusive and displacive mechanisms, resulting in a sluggish dynamics after yield. Further investigations are required to better understand and characterize this deformation mode, and to determine the critical NP size above which dislocation nucleation and propagation occur. At last we find that the strength depends on the NP shape, and is higher than the theoretical bulk strength but clearly lower than predictions from classical MD calculations of larger systems, hinting that strength stops increasing below a size threshold.

Acknowledgements

Computer time for this study was partially provided by the MCIA (Mésocentre de Calcul Intensif Aquitain).This work pertains to the French Government program "Investissements d'Avenir" (EUR INTREE, reference ANR-18-EURE-0010, and LABEX INTERACTIFS, reference ANR-11-LABX-0017-01).

Declaration of competing interest

The authors declare that they have no known competing financial interests or personal relationships that could have appeared to influence the work reported in this paper.

References

[1] G. F. Taylor, A method of drawing metallic filaments and a discussion of their properties and uses, Phys. Rev. 23 (5) (1924) 655–660. doi:10.1103/physrev.23.655.

[2] S. S. Brenner, Tensile strength of whiskers, J. Appl. Phys. 27 (12) (1956) 1484–1491. doi:10.1063/1.1722294.

[3] J. Pokluda, M. Černý, P. Šandera, M. Šob, Calculations of theoretical strength: State of the art and history, J. Computer-Aided Mater. Des. 11 (1) (2004) 1–28. doi:10.1007/s10820-004-4567-2.

[4] A. Sharma, J. Hickman, N. Gazit, E. Rabkin, Y. Mishin, Nickel nanoparticles set a new record of strength, Nature Communications 9 (1) (2018) 4102.

[5] A. Sharma, R. Kositski, O. Kovalenko, D. Mordehai, E. Rabkin, Giant shape- and size-dependent compressive strength of molybdenum nano- and microparticles, Acta Mater. 198 (2020) 72–84. doi:10.1016/j.actamat.2020.07.054.

[6] W.-Z. Han, L. Huang, S. Ogata, H. Kimizuka, Z.-C. Yang, C. Weinberger, Q.-J. Li, B.-Y. Liu, X.-X. Zhang, J. Li, E. Ma, Z.-W. Shan, From "smaller is stronger" to "size-independent strength plateau": Towards measuring the ideal strength of iron, Adv. Mater. 27 (22) (2015) 3385–3390. doi:10.1002/adma.201500377.

[7] S. Azadehranjbar, R. Ding, I. M. P. Espinosa, A. Martini, T. D. B. Jacobs, Size-dependent role of surfaces in the deformation of platinum nanoparticles, ACS Nano (apr 2023). doi:10.1021/acsnano.2c11457.

[8] J. Amodeo, K. Lizoul, Mechanical properties and dislocation nucleation in nanocrystals with blunt edges, Materials & Design 135 (2017) 223 – 231. doi:https://doi.org/10.1016/j.matdes.2017.09.009.

[9] D. Kilymis, C. Gérard, J. Amodeo, U. Waghmare, L. Pizzagalli, Uniaxial compression of silicon nanoparticles: An atomistic study on the shape and size effects, Acta Mater. 158 (2018) 155–166. doi:10.1016/j.actamat.2018.07.063.

[10] J. Zimmerman, A. Bisht, Y. Mishin, E. Rabkin, Size and shape effects on the strength of platinum nanoparticles, J. Mater. Sci. 56 (32) (2021) 18300–18312. doi:10.1007/s10853-021-06435-7.

[11] J. Amodeo, L. Pizzagalli, Modeling the mechanical properties of nanoparticles: a review, Comptes Rendus Physique 22 (S3) (2021) 1–32. doi:10.5802/crphys.70.

[12] Y. Feruz, D. Mordehai, Towards a universal size-dependent strength of face-centered cubic nanoparticles, Acta Mater. 103 (2016) 433 – 441. doi:http://dx.doi.org/10.1016/j.actamat.2015.10.027.

[13] L. Yang, J.-J. Bian, G.-F. Wang, Impact of atomic-scale surface morphology on the size-dependent yield stress of gold nanoparticles, J. Phys. D: Appl. Phys. 50 (2017) 245302.

[14] S. Bel Haj Salah, Plasticity of face centered cubic metallic nanoparticles, Ph.D. thesis, Ecole Nationale Supérieure de Mécanique et d'Aérotechnique (2018).

[15] P. Giannozzi, O. Andreussi, T. Brumme, O. Bunau, M. B. Nardelli, M. Calandra, R. Car, C. Cavazzoni, D. Ceresoli, M. Cococcioni, N. Colonna, I. Carnimeo, A. D. Corso, S. de Gironcoli, P. Delugas, R. A. DiStasio, A. Ferretti, A. Floris, G. Fratesi, G. Fugallo, R. Gebauer, U. Gerstmann, F. Giustino, T. Gorni, J. Jia, M. Kawamura, H.-Y. Ko, A. Kokalj, E. Küçükbenli, M. Lazzeri, M. Marsili, N. Marzari, F. Mauri, N. L. Nguyen, H.-V. Nguyen, A. O. de-la Roza, L. Paulatto, S. Poncé, D. Rocca, R. Sabatini, B. Santra, M. Schlipf, A. P. Seitsonen, A. Smogunov, I. Timrov, T. Thonhauser, P. Umari, N. Vast, X. Wu, S. Baroni, Advanced capabilities for materials modelling with quantum ESPRESSO, J. Phys.: Condens. Matter 29 (46) (2017) 465901. doi:10.1088/1361-648x/aa8f79.

[16] L. Pizzagalli, First principles molecular dynamics calculations of the mechanical properties of endofullerenes containing noble gas atoms or small molecules, Phys. Chem. Chem. Phys. 24 (16) (2022) 9449–9458. doi:10.1039/d2cp00622g.

[17] L. Pizzagalli, Mechanical properties of c60 at finite temperature from first-principles calculations, Diamond & Related Materials 123 (2022) 108870. doi:10.1016/j.diamond.2022.108870.
[18] L. Pizzagalli, J. Godet, Ultra high strength and plasticity mechanisms of si and sic nanoparticles revealed by first principles molecular dynamics (2023). arXiv:2310.11170.
[19] M. Methfessel, A. T. Paxton, High-precision sampling for brillouin-zone integration in metals, Phys. Rev. B 40 (1989) 3616–3621. doi:10.1103/PhysRevB.40.3616.
[20] J. P. Perdew, K. Burke, M. Ernzerhof, Generalized gradient approximation made simple, Phys. Rev. Lett. 77 (18) (1996) 3865–3868.
[21] P. E. Blöchl, Projector augmented-wave method, Phys. Rev. B 50 (1994) 17953–17979. doi:10.1103/PhysRevB.50.17953.
[22] L. Pizzagalli, Finite-temperature mechanical properties of nanostructures with first-principles accuracy, Phys. Rev. B 102 (9) (2020) 094102.
[23] G. Bussi, D. Donadio, M. Parrinello, Canonical sampling through velocity rescaling, J. Chem. Phys. 126 (1) (2007) 014101. doi:10.1063/1.2408420.
[24] J. Li, The mechanics and physics of defect nucleation, Mater. Res. Soc. Bull. 32 (2007) 151–159.
[25] J. Sun, L. He, Y.-C. Lo, T. Xu, H. Bi, L. Sun, Z. Zhang, S. X. Mao, J. Li, Liquid-like pseudoelasticity of sub-10-nm crystalline silver particles, Nature Materials 13 (11) (2014) 1007–1012. doi:10.1038/nmat4105.
[26] J. Wan, Y. L. Fan, D. W. Gong, S. G. Shen, X. Q. Fan, Surface relaxation and stress of fcc metals: Cu, ag, au, ni, pd, pt, al and pb, Modelling and Simulation in Materials Science and Engineering 7 (2) (1999) 189–206. doi:10.1088/0965-0393/7/2/005.
[27] R. Ahlrichs, S. D. Elliott, Clusters of aluminium, a density functional study, Phys. Chem. Chem. Phys. 1 (1) (1999) 13–21. doi:10.1039/a807713d.
[28] B. Molleman, T. Hiemstra, Size and shape dependency of the surface energy of metallic nanoparticles: unifying the atomic and thermodynamic approaches, Phys. Chem. Chem. Phys. 20 (31) (2018) 20575–20587. doi:10.1039/c8cp02346h.
[29] W. Li, T. Wang, *Ab initio* investigation of the elasticity and stability of aluminium, J. Phys.: Condens. Matter 10 (43) (1998) 9889–9904. doi:10.1088/0953-8984/10/43/033.
[30] P. Mahler Larsen, S. Schmidt, J. Schiøtz, Robust structural identification via polyhedral template matching, Modelling Simul. Mater. Sci. Eng. 24 (5) (2016) 055007. doi:10.1088/0965-0393/24/5/055007.
[31] S. Bel Haj Salah, C. Gerard, L. Pizzagalli, Influence of surface atomic structure on the mechanical response of aluminum nanospheres under compression, Comp. Mat. Sci. 129 (2017) 273–278. doi:10.1016/j.commatsci.2016.12.033.
[32] D. Mordehai, S.-W. Lee, B. Backes, D. J. Srolovitz, W. D. Nix, E. Rabkin, Size effect in compression of single-crystal gold microparticles, Acta Mater. 59 (13) (2011) 5202 – 5215. doi:10.1016/j.actamat.2011.04.057.
[33] S. Ogata, J. Li, S. Yip, Ideal pure shear strength of aluminum and copper, Science 298 (5594) (2002) 807–811. doi:10.1126/science.1076652.
[34] D. M. Clatterbuck, C. R. Krenn, M. L. Cohen, J. W. Morris, Phonon instabilities and the ideal strength of aluminum, Phys. Rev. Lett. 91 (13) (2003) 135501. doi:10.1103/physrevlett.91.135501.
[35] R. Yang, B. Tang, T. Gao, A comparison of mechanical properties between al and al_3mg, Int. J. of Mod. Phys. B 30 (01) (2016) 1550243. doi:10.1142/s0217979215502434.
[36] L. Piot, S. L. Floch, T. Cornier, S. Daniele, D. Machon, Amorphization in nanoparticles, J. Phys. Chem. C 117 (21) (2013) 11133–11140. doi:10.1021/jp401121c.